Journal of Materials Chemistry A

Blade-coated Highly Efficient Thick Active Layer of Non-fullerene Organic Solar Cells

Journal:	*Journal of Materials Chemistry A*
Manuscript ID	TA-COM-09-2019-009799.R1
Article Type:	Communication
Date Submitted by the Author:	20-Sep-2019
Complete List of Authors:	Zhang, Lin; Xi'an Jiaotong University, State Key Laboratory for Mechanical Behavior of Materials; Central South University, Hunan Key Laboratory for Super Microstructure and Ultrafast Process, School of Physics and Electronics Zhao, Heng; Xi'an Jiaotong University, State Key Laboratory for Mechanical Behavior of Materials Lin, Baojun; Xi'an Jiaotong University, State Key Laboratory for Mechanical Behavior of Materials Yuan, Jian; Xi'an Jiaotong University, State Key Laboratory for Mechanical Behavior of Materials Xu, Xianbin; Xi'an Jiaotong University, State Key Laboratory for Mechanical Behavior of Materials Wu, Jingnan ; Soochow University, State and Local Joint Engineering Laboratory for Novel Functional Polymeric Materials, Laboratory of Advanced Optoelectronic Materials, College of Chemistry, Chemical Engineering and Materials Science Zhou, Ke; Xi'an Jiaotong University, State Key Laboratory for Mechanical Behavior of Materials Guo, Xia; Soochow University, State and Local Joint Engineering Laboratory for Novel Functional Polymeric Materials, Laboratory of Advanced Optoelectronic Materials, College of Chemistry, Chemical Engineering and Materials Science Zhang, Maojie; Soochow University, State and Local Joint Engineering Laboratory for Novel Functional Polymeric Materials, Laboratory of Advanced Optoelectronic Materials, College of Chemistry, Chemical Engineering and Materials Science Ma, Wei; Xi'an Jiaotong University, State Key Laboratory for Mechanical Behavior of Materials

ARTICLE

Blade-coated Highly Efficient Thick Active Layer of Non-fullerene Organic Solar Cells

Received 00th January 20xx,
Accepted 00th January 20xx

DOI: 10.1039/x0xx00000x

Lin Zhang, [ab] Heng Zhao, [a] Baojun Lin, [a] Jian Yuan, [a] Xianbin Xu, [a] Jingnan Wu, [c] Ke Zhou, [a] Xia Guo, [c] Maojie Zhang [c] and Wei Ma*[a]

Regulating molecular ordering and nanoscale morphology of photoactive layer is crucial to achieve high carrier mobility in fabricating thick-film organic solar cells (OSCs). Herein, molecular ordering and phase separation were finely controlled by varying substrate temperature in blade-coated PM6:IT-4F devices. The blade-coated devices with low substrate temperature (30 °C) show low crystallinity of IT-4F and poor device performance. However, high power conversion efficiency (PCE) of 13.64% was achieved for the blade-coated device at 50 °C in air without any other processing treatments, due to the well-ordered molecular packing along the backbone direction of IT-4F molecules. When the film-thickness increased to 400 nm, an excellent PCE of 10.22% was achieved in the blade-coated device at 70 °C, which is higher than the optimal blade-coated device at 50 °C. It was attributed to the much improved crystallinity within the long-range ordered side-chain packing of IT-4F molecules and the newly emerged small-scale phase separation providing purer domains and continuous charge transport channels. Furthermore, the large-area (90 mm^2) devices exhibit high PCEs of 11.39% and 9.76% with a 56 mm^2 aperture at the film thickness of 135 nm and 306 nm, respectively. In addition, the blade-coated device at 70 °C exhibits good storage stability. This work provides comprehensive guidance for optimizing molecular ordering and nanoscale morphology in fabricating high-efficient thick-film OSCs.

Introduction

Non-fullerene organic solar cells (OSCs)[1-4] have attracted considerable attention in recent years and power conversion efficiency (PCE) over 16% has been achieved in single-junction binary device.[5] However, these progresses are made by spin-coating on small-area devices,[6, 7] which are material wasteful and difficult to extend to mass production.[8] Therefore, developing large-area production technology is of great needed. Fortunately, as a continuously coating technology, slot-die coating exhibits excellent compatibility with large-area roll-roll coating.[9-14] Meanwhile, blade-coating severing as a prototype tool of slot-die coating possesses similar features,[8, 15] so it's suitable for early experimental studies in the lab. Encouragingly, the blade-coated OSCs have made great progresses with the PCE over 12%.[16-19] Even so, an important challenge for achieving high performance in the thick-film devices by blade-coating exists,[20] where most efficient new materials exhibit optimal photovoltaic performance with a film-thickness of about 100 nm. It is difficult to maintain good reproducibility during the fast fabrication of pin-hole-free large-area OSCs at this film-thickness.[21] Increasing the film-thickness can alleviate the phenomenon of pin-hole-free and benefit to fabricate homogeneous large-area films. However, carrier mobility is of great importance to fabricate thick-film device. In order to achieve high performance in the thick-film device, high carrier mobilities are of great desire for the fast charge transfer and low recombination loss.[22-24]

In the field of organic semiconductor, molecular ordering greatly impacts the electronic and optoelectronic properties.[25-27] Fine control of molecular ordering is considered as an efficient approach to achieve fast charge transport, so as to obtain great performance.[26-29] Sirringhaus et al reported that the mobility of poly(3-hexylthiophene)-based field-effect transistor with edge-on molecular packing respect to the substrate is over 100 times than that of the face-on molecular packing.[26] In addition, Carpenter et al reported the competition between exceptionally long-rang alkyl side-chain ordering and backbone ordering in semiconducting polymers and its impact on electronic and optoelectronic properties. It was demonstrated that the long-range side-chain ordering with atypical edge-on texture exhibits 2.5 times improved field-effect transistor mobility as compared to the corresponding backbone ordering.[25] Furthermore, Li et al achieved high mobility by film-casting with spin-coating on a hot substrate.[27]

[a] State Key Laboratory for Mechanical Behavior of Materials, Xi'an Jiaotong University, Xi'an 710049, China. E-mail: msewma@xjtu.edu.cn
[b] Hunan Key Laboratory for Super Microstructure and Ultrafast Process, School of Physics and Electronics, Central South University, Changsha 410083, China.
[c] State and Local Joint Engineering Laboratory for Novel Functional Polymeric Materials, Laboratory of Advanced Optoelectronic Materials, College of Chemistry, Chemical Engineering and Materials Science, Soochow University, Suzhou 215123, China.

Electronic Supplementary Information (ESI) available: [details of any supplementary information available should be included here]. See DOI: 10.1039/x0xx00000x

It reported that spin-coating on a hot substrate can reduce molecular organization time, and then suppress the crystallization. Furthermore, it leads to the change of molecular packing from flat-on and edge-on lamellar crystallization to both *H*- and *J*-type face-on π-π stacking of small molecules in a more condensed state as compared to the spin-coating without hot substrate. Thus, high carrier mobility and excellent PCE (13.8%) were achieved. Nevertheless, fine controlling substrate temperature in spin-coating process is difficult, and spin-coating is incompatible with large-area roll-roll coating. It is worth to note that the blade-coating can inherently induce high degree of molecular packing for conjugated polymer and small molecule, which benefit to improve charge transport.[17, 30, 31] However, fine controlling molecular ordering and phase separation by varying the substrate temperature to improve carrier mobility in blade-coating high performance thick-film OSCs is not exploited.

In this work, molecular ordering and phase separation were finely controlled by varying substrate temperature in blade-coated PM6:IT-4F OSCs. It was demonstrated that blade-coating at the substrate temperature of 30 °C (blade-coating @30 °C) shows low crystallinity of IT-4F which is similar with the spin-coating. However, a great PCE of 13.64% is achieved for the blade-coated @50 °C device, and the blade-coated @70 °C device shows a high PCE of 10.22% at the film-thickness above 400 nm. Furthermore, the large-area (90 mm^2) devices were fabricated, and obtained high PCEs of 11.39% and 9.76% with a 56 mm^2 aperture at the film thickness of 135 nm and 306 nm, respectively. In addition, the blade-coated @70 °C device exhibits good storage stability.

Results and discussion

Due to the high performance of PM6:IT-4F based OSCs and the lower electron mobility than hole mobility, the PM6:IT-4F system was selected in this work. The chemical structures of PM6 and IT-4F are present in Fig. 1a,[32-36] and Fig. 1b is the diagrammatic drawing of blade-coating with the heating substrate. The UV-vis absorption spectra exhibit excellent complementarity between the neat PM6 and IT-4F films (Fig. 1c). According to the normalized absorption spectra at 0-1 transition peaks (578 nm for PM6 and 664 nm for IT-4F), both blade-coated PM6 and IT-4F films exhibit enhanced 0-0 transition peaks (619 nm for PM6 and 724 nm for IT-4F) than the corresponding spin-coated films, suggesting the stronger aggregation and ordering for the blade-coated films.[37] The inset is the energy level of PM6:IT-4F system, of which the highest occupied molecular orbital and lowest unoccupied molecular orbital levels are -5.50 eV/-3.61 eV for PM6, and -5.69 eV/-4.07 eV for IT-4F, respectively.[34, 35] Grazing incident wide-angle X-ray scattering (GIWAXS)[38] are employed to explore the molecular ordering and crystallization. Fig. 1d gives the crystallization coherence length (CCL) of lamellar stacking obtained from the GIWAXS results (Fig. S1) by fitting the (100) peak in the in-plane direction according to the Scherrer equation, which indicates the mean size of ordered (crystalline) domains.[39, 40] The calculated CCL values of spin-coated PM6 and IT-4F are 6.14 nm and 2.74 nm, respectively. However, for the corresponding blade-coated films, the CCL values increase to 6.35 nm and 2.86 nm, respectively, revealing that blade-coating can induce higher degree of molecular packing for both of PM6 and IT-4F, which is well matched with the absorption spectra (Fig. 1c). The improved crystallization for blade-coated films is beneficial to fabricate high performance devices.

Bulk-heterojunction organic solar cells with the device configuration of ITO/PEDOT:PSS (poly(3,4-ethylenedioxythiophene):poly(styrenesulfonate)/ PM6:IT-4F/ZrAcac (zirconium acetylacetonate)/Al were fabricated by spin-coating and blade-coating in ambient environment without any other processing treatments.[41] The effective device area is 4 mm^2 and the optimal film-thickness is kept at 100-140 nm. For the blade-coated devices, the substrate was heated by a controlled heater to keep the substrate temperature at 30 °C, 50 °C and 70 °C (named as blade-coating @30 °C, blade-coating @50 °C and blade-coating @70 °C), respectively. The current density-voltage (*J-V*) characteristics are shown in Fig. 2a, and the photovoltaic parameters are summarized in Table 1. The spin-coated devices exhibit an average PCE of 11.78% with the open-circuit voltage (V_{oc}) of 0.88 V, short-circuit current (J_{sc}) of 18.99 mA cm^{-2} and fill factor (FF) of 70.47%. For the blade-coated @30 °C devices, the average PCE, V_{oc}, J_{sc} and FF are 11.83%, 0.87 V, 19.89 mA cm^{-2} and 68.39%, respectively. As the substrate temperature increases to 50 °C, the corresponding devices exhibit an average PCE of 13.15% with a highest PCE of 13.64%, due to the improved J_{sc} (20.76 mA cm^{-2}) and FF (72.00%). However, a further increased substrate temperature (70 °C) leads to a slightly decrease of device performance with the PCE of 13.24%. The current density integrated from EQE curves (Fig. 2b) are 18.71 mA cm^{-2}, 19.30 mA cm^{-2}, 20.09 mA cm^{-2} and 20.14 mA cm^{-2} for the devices of spin-coating, blade-coating @30 °C, blade-coating @50 °C and blade-coating @70 °C, respectively, which are consistent with the current density obtained from *J-V* measurements.

The charge carrier mobilities were investigated by space charge limited current (SCLC) model.[42, 43] As shown in Fig. S2, Fig. 2c and Table 1, all these three blade-coated devices exhibit much higher hole mobilities than the spin-coated device, and the device of blade-coating @50 °C presents the highest hole mobility of 3.76×10^{-4} cm^2 V^{-1} s^{-1}. On the other hand, the electron mobility of blade-coated @30 °C device shows slight improvement as compared with the corresponding spin-coated device. When the substrate temperature increases from 30 °C to 50 °C, the electron mobility increases from 1.31×10^{-4} to 3.52×10^{-4} cm^2 V^{-1} s^{-1}. In addition, further increase of the substrate temperature to 70 °C does not result in the continuous enhancement of electron mobility (3.41×10^{-4} cm^2 V^{-1} s^{-1}). Notably, the devices of blade-coating @50 °C and blade-coating @70 °C exhibit high and balanced carrier mobilities which benefit to improve charge transport and suppress recombination loss, so as to improve the photovoltaic performance. In order to analyze the variation of photovoltaic performance, the charge carrier dynamics involving exciton dissociation, charge extraction and collection processes are investigated.[44-47] Fig. 2d shows the plots of photocurrent

density (J_{ph}) versus the effective voltage (V_{eff}) of various devices.[44] J_{ph} is defined by the equation of $J_{ph}=J_L-J_D$, where J_L and J_D are the current density under light illumination (AM 1.5G, 100 mW cm^{-2}) and in the dark, respectively. V_{eff} is defined by the equation of $V_{eff}=V_0-V_a$, where V_0 is the voltage at J_{ph}=0, and V_a is the applied voltage. The exciton dissociation probability (P) is determined by $P=J_{ph}/J_{sat}$ at short-circuit condition, where the J_{sat} is the saturation photocurrent density at high V_{eff} value. The calculated exciton dissociation probabilities[44] for the devices of spin-coating, blade-coating @30 °C, blade-coating @50 °C and blade-coating @70 °C are 97.79%, 96.83%, 98.83% and 97.49%, respectively. The large value of P for the device of blade-coating @50 °C indicates an excellent charge collection and extraction, which well matches the high FF of 72.00%. Meanwhile, the dependence of V_{oc} and J_{sc} on the light intensity was employed to investigate the recombination mechanism.[45, 46] The semilogarithmic plot of V_{oc} as a function of light intensity delivers a linear relationship with a slop of kT/q, where the small slop of kT/q indicates the low Shockley-Read-Hall (SRH) recombination.[46] As displayed in the Fig. 2d, the small slope of 1.36 kT/q suggests the low SRH recombination for the device of blade-coating @50 °C. In addition, according to the relationship of $J_{sc}\propto$(light intensity)$^{\alpha}$, the fitted slopes (α) (Fig. 2f) are 0.97, 0.97, 0.98 and 0.97 for the devices of spin-coating, blade-coating @30 °C, blade-coating @50 °C and blade-coating @70 °C, respectively, where α=1 means that all dissociated free carriers are collected at corresponding electrodes.[46] The device of blade-coating @50 °C present large values of α=0.98, suggesting the weak bimolecular recombination. Consequently, the excellent photovoltaic performance for the devices of blade-coating @50 °C (PCE=13.15%) can be attributed to the high and balanced carrier mobilities, as well as the low recombination with high exciton dissociation efficiency and charge collection efficiency, which should be related to the nanoscale morphology of active layer.

To understand the variation of photovoltaic performance, the morphology characterization of resonant soft X-ray scattering (RSoXS)[48, 49] and transmission electron microscopy (TEM) was carried out. The RSoXS is a widely used method to characterize the phase separation of active layer in OSCs, of which an X-ray energy of 284.8 eV was selected due to the high scattering contrast between PM6 and IT-4F. As shown in Fig. 3a, Fig. S3 and Table 2, the spin-coated film possesses a domain size of 28 nm, and the blade-coated @30 °C film shows a similar domain size of 30 nm. However, the domain sizes of blade-coated @50 °C and blade-coated @70 °C films increase to 39 nm and 41 nm, respectively. Notably, another small length-scale of phase separation with the domain size of 13 nm (domain spacing 26 nm) at q=0.23 nm^{-1} was observed in the blade-coated @70 °C film by fitting the profile with lognormal model (Fig. 3a). In addition, the calculated relative purities about these four films are 0.84, 0.87, 0.93 and 1, respectively, where the high purity is considered to be beneficial for improving charge transport and decreasing recombination losses.[50-52] The change of domain size and the increased purity with the increased substrate temperature may arise from the variation of molecular packing and crystallization, which will be discussed below. Due to the low material constrast of TEM characterization, homogeneous films without obvious nanostructure are present in the TEM images of spin-coated film (Fig. 3b), blade-coated @30 °C film (Fig. 3c) and blade-coated @50 °C film (Fig. 3d). However, lots of fiber structures can be obviously observed through the whole film in the blade-coated @70 °C film (Fig. 3e), indicative of the high crystallinity, which maybe the reason of the highest domain purity for the blade-coated @70 °C film.

In order to investigate the detailed information of molecular ordering and crystallization behavior, GIWAXS[38] measurements for the PM6:IT-4F films were performed. As shown in Fig. 4, all the PM6:IT-4F films exhibit pronounced (010) scattering peak at q=1.67 Å^{-1} in the out-of-plane direction, which originates from the π-π stacking of PM6, suggesting the strong face-on orientation. However, IT-4F in the four blend films presents broad (010) diffracting peaks at q≈1.42 Å^{-1} in both in-plane and out-of-plane direction, indicating the existence of both face-on and edge-on orientation. Notably, the scattering peaks at low q location show the more pronounced difference for these four films, and the corresponding structure parameters obtained by fitting the GIWAXS profiles (Fig. S4) are shown in Table 3 and Table S1. The calculated CCL[39] of PM6 for spin-coated blend film in the in-plane and out-of-plane direction are 10.66 and 9.27 nm with the corresponding d-spacing of 2.09 and 2.17 nm, respectively. For the blade-coated films, the d-spacing of PM6 has almost no change, but CCL shows varying degrees of increase, suggesting the improved crystallinity of PM6 for the blade-coated films, especially for the blade-coated @50 °C film (CCL=16.62 nm, 10.30 nm) and blade-coated @70 °C film (CCL=13.24 nm, 10.70 nm). There are no pronounced scattering peaks of IT-4F at low q location in the spin-coated film and blade-coated @30 °C film, indicating the low crystallinity of IT-4F in the blend film. Generally, the charge transport in crystalline domain is faster than the amorphous domain.[53, 54] Thus, the low crystallinity of IT-4F may be the reason why the electron mobility of these two corresponding devices is low (Fig. 2c).

Inspiringly, a new and pronounced scattering peak appears in the in-plane direction at q=0.31 Å^{-1} for the blade-coated @50 °C film, suggesting the existence of another structural ordering. The newly appeared scattering peak with a lattice constant of 2.03 nm (CCL=19.49 nm) is attributed to the molecular ordering of IT-4F along the backbone which is named as backbone packing.[25, 55] The backbone packing can effectively extend the electron transport pathway and therefore significantly improve the carrier mobility, so as to improve photovoltaic performance.[55] Surprisingly, the (001) scattering peak of backbone packing disappears in the blade-coated @70 °C film together with multiple sharp scattering peaks emerged in both in-plane and out-of-plane direction, demonstrating a much higher degree of crystallinity, compared with other three blend films. As evidenced by the GIWAXS data of pure IT-4F (Fig. S1), the sharp scattering peak at q=0.39 Å^{-1} in both in-plane and out-of-plane direction should be the (100) scattering peak of IT-4F, indicative of side-chain packing (lamellar packing), suggesting the much high crystallinity of IT-4F with both face-on and edge-on orientation. Interestingly, according to the fitting results, the

calculated CCL of in-plane (100) scattering peak for IT-4F is 26.91 nm, which approximates the domain spacing (26 nm) of the appeared another length-scale phase separation (Fig. 3a), indicating that the newly appeared phase separation may attributes to the scattering contrast between lamellar crystal and the surrounding region.

Generally, the lamellar packing by side-chain is considered to be a thermodynamic steady state, and other molecule packing is intermediate state which is unsteady, such as face-on π-π stacking and backbone stacking.[25] For the blade-coated @70 °C film, the high substrate temperature provides enough energy and accelerates the movement of IT-4F molecules. It facilitates the molecular ordering, so it is easy to reach the steady state of lamellar packing with side-chain. For the spin-coated film and blade-coated @30 °C film, IT-4F molecules move slowly in the blend films, and it is difficult to facilitate the molecule packing, resulting in the weak crystallinity. However, in the blade-coated @50 °C film, moderate substrate temperature can trigger the movement and arrangement of IT-4F molecules, but it's not enough to reach the steady state. Thus, an intermediate state of backbone packing for IT-4F molecules is formed, where the charge transport along the backbone packing is fast, resulting in the high electron mobility. Hence, the backbone packing in the blade-coated @50 °C film and the enhanced side-chain packing in blade-coated @70 °C film lead to the improved electron mobility, so as to achieve high PCEs of 13.64% and 13.24%.

Considering the improved charge carrier mobilities and photoelectric properties, thick films were fabricated， which are beneficial for the production of pin-hole-free large-area OSCs. The photovoltaic performance of PM6:IT-4F based devices with different thicknesses are shown in Fig. 5a, Fig. S5 and Table S2. The optimal thicknesses of spin-coated device, blade-coated @30 °C device, blade-coated @50 °C device and blade-coated @70 °C device are 103, 132, 134, and 141 nm, respectively, where the increased optimal thickness attributes to the improved and balanced carrier mobilities. When the film-thickness increased, the V_{oc} and FF have all decreased variously, while the J_{sc} and PCE increase first and then decrease. However, the blade-coated @70 °C device decreases more slowly than the other three devices as the film-thickness increased, resulting a higher photovoltaic performance at the thickness >230 nm than other three devices. Impressively, the blade-coated @70 °C device shows a notable PCE of 10.22% at the film-thickness of 400 nm, which is one of the highest values for the thick-film devices at present. As shown in Fig. 5b, the J_{sc} of blade-coated @50 °C device and blade-coated @70 °C device are 15.31 and 18.91 mA cm^{-2}, and both of them are far from the saturated current density at the bias voltage of -2 V, indicating the low exciton dissociation efficiency and charge extraction efficiency in the thick-film devices. However, the blade-coated @70 °C device shows smaller difference of current density between the open-circuit condition and the bias voltage of -2 V than the blade-coated @50 °C device, suggesting the high exciton dissociation efficiency and charge extraction efficiency for the blade-coated @70 °C device at the film-thickness of ~500 nm.[56] The approximate exciton dissociation probability obtained from J_{ph}-V_{eff} curves (Fig. 5c) are about 68.58% and 78.88%, further demonstrating the better exciton dissociation and charge extraction for the blade-coated @70 °C device.[46] Furthermore, the plot of V_{oc} versus light intensity (Fig. 5d) shows less recombination loss for the blade-coated @70 °C device due to the low value of 1.72 kT/q than that of blade-coated @50 °C device, which well matches with the high photovoltaic performance for the thick-film device.

The nanoscale morphology of thick film was investigated by GIWAXS and RSoXS. As shown in Fig. S6, the thick film shows similar morphological characteristic with the thin film, except for the slightly increased domain size (from 39 nm to 44 nm), indicating that the film-thickness has negligible effect on the morphology for the blade-coated PM6:IT-4F film. Notably, the blade-coated @50 °C device exhibits the higher PCE than the blade-coated @70 °C device at the thickness of about 130-140 nm. However, when the film thickness is about >400 nm, the blade-coated @50 °C device presents lower PCE than the blade-coated @70 °C device. The reason should be that the backbone packing (d-spacing is 2.03 nm and CCL is 19.49 nm in Table 3) in blade-coated @50 °C film is a short-range order, which is more difficult to form continuous and efficient transport channels in thick film than in thin film. On the other hand, the side-chain packing (d-spacing is 1.61 nm and CCL is 26.91 nm in Table 3) in the blade-coated @70 °C film is a long-range order, which is more suitable to fabricate thick-film device. Moreover, the newly appeared small-scale phase region in the blade-coated @70 °C film should play more important role in thick film for efficient charge transport. Therefore, the blade-coated @70 °C device possesses higher PCE than the corresponding blade-coated @50 °C device at the film-thickness of about 500 nm.

The large-area devices of 90 mm^2 device area with various film thickness were also fabricated by blade-coating at the substrate temperature of 70 °C in ambient environment. The *J-V* measurement of large-area device was made with an aperture (or mask) of 56 mm^2. As shown in Fig. 5e, Fig. S7 and Table S3, the device with 135 nm active layer exhibits a highest PCE of 11.39% and an average PCE of 10.77% with the V_{oc} of 0.83 V, J_{sc} of 19.28 mA cm^{-2} and FF of 67.56%. Although the PCE and FF decreased as the film thickness increased, the large-area thick device with the thickness of 306 nm exhibits a highest PCE of 9.76%. In addition, the long term stability of blade-coated @70 °C device was investigated. As shown in Fig. 5f, after 1344 h of storage in N_2-filled glovebox, the PCE damage is only about 6%, indicating considerable long-term stability. The high device performance of blade-coated large-area thick-film OSC and considerable device stability exhibit great potential in the industrial production and commercial application of organic solar cells.

Conclusions

In summary, we fabricated organic solar cells based on PM6:IT-4F blend by blade-coating at different substrate temperature in air, and the devices with various film-thicknesses were also prepared. It was demonstrated that the film-thickness has little effect on the morphology of active layer. In addition, the blade-coated @30 °C device shows a PCE of 12.25% which

approximates to that of spin-coated device, due to their similar morphology characteristic with low crystallinity of IT-4F. A highest PCE of 13.64% was achieved for the blade-coated @50 °C device, due to the newly appeared backbone packing of IT-4F molecules, accompanied by the improvement of electron mobility. However, the backbone packing is short-range order which is more difficult to form continuous and efficient transport channels in thick film than thin film. Thus, this molecule packing is unsuitable to fabricate thick-film devices, where the PCE is only 7.19% at the film-thickness of about 500 nm. When the substrate temperature increase to 70 °C, the IT-4F molecules move faster and tend to form steady state of side-chain packing, which is long-range order and suitable to fabricate thick-film device. Moreover, the blade-coated @70 °C film appears another small-scale phase separation which plays much important role in thick film for continuous charge transport channels. Hence, a high PCE of 10.22% was achieved for the blade-coated @70 °C device with film-thickness of about 400 nm, which is much higher than the corresponding blade-coated @50 °C device. Furthermore, the large-area (90 mm^2) device exhibits high PCEs of 11.39% and 9.76% with a 56 mm^2 aperture at the film thickness of 135 nm and 306 nm, respectively. In addition, the blade-coated device at 70 °C exhibits good storage stability with respect to the efficiency. This work reports an efficient approach to achieve high mobility by controlling molecular ordering, which can be employed to other similar non-fullerene systems with low electron mobility of small molecular acceptor, showing great prospect in the large-area fabrication of high-efficiency and thick-film non-fullerene OSCs.

Conflicts of interest

There are no conflicts to declare.

Acknowledgements

Thanks for the support from Ministry of science and technology (No. 2016YFA0200700), NSFC (21704082, 21875182, 21534003), China Postdoctoral Science Foundation (2017M623162), 111 project 2.0 (BP2018008). X-ray data was acquired at beamlines 7.3.3 and 11.0.1.2 at the Advanced Light Source, which is supported by the Director, Office of Science, Office of Basic Energy Sciences, of the U.S. Department of Energy under Contract No. DE-AC02-05CH11231. The authors thank Chenhui Zhu at beamline 7.3.3, and Cheng Wang at beamline 11.0.1.2 for assistance with data acquisition.

References

1. J. H. Hou, O. Inganas, R. H. Friend and F. Gao, *Nat. Mater.*, 2018, **17**, 119-128.
2. A. Kuzmich, D. Padula, H. B. Ma and A. Troisi, *Energy Environ. Sci.*, 2017, **10**, 395-401.
3. S. S. Chen, S. M. Lee, J. Q. Xu, J. Lee, K. C. Lee, T. Y. Hou, Y. K. Yang, M. Jeong, B. Lee, Y. Cho, S. Jung, J. Oh, Z. G. Zhang, C. F. Zhang, M. Xiao, Y. F. Li and C. Yang, *Energy Environ. Sci.*, 2018, **11**, 2569-2580.
4. X. L. Ma, W. Gao, J. S. Yu, Q. S. An, M. Zhang, Z. H. Hu, J. X. Wang, W. H. Tang, C. L. Yang and F. J. Zhang, *Energy Environ. Sci.*, 2018, **11**, 2134-2141.
5. B. Fan, D. Zhang, M. Li, W. Zhong, Z. Zeng, L. Ying, F. Huang and Y. Cao, *Sci. China Chem.*, 2019, **62**, 746-752.
6. Y. Xie, F. Yang, Y. Li, M. A. Uddin, P. Bi, B. Fan, Y. Cai, X. Hao, H. Y. Woo, W. Li, F. Liu and Y. Sun, *Adv. Mater.*, 2018, **30**, 1803045.
7. Y. Xie, L. Huo, B. Fan, H. Fu, Y. Cai, L. Zhang, Z. Li, Y. Wang, W. Ma, Y. Chen and Y. Sun, *Adv. Funct. Mater.*, 2018, **28**, 1800627.
8. H. W. Ro, J. M. Downing, S. Engmann, A. A. Herzing, D. M. DeLongchamp, L. J. Richter, S. Mukherjee, H. Ade, M. Abdelsamie, L. K. Jagadamma, A. Amassian, Y. H. Liu and H. Yan, *Energy Environ. Sci.*, 2016, **9**, 2835-2846.
9. J.-W. Lee, D.-K. Lee, D.-N. Jeong and N.-G. Park, *Adv. Funct. Mater.*, 2018, **2**, 1807047.
10. F. Liu, S. Ferdous, E. Schaible, A. Hexemer, M. Church, X. D. Ding, C. Wang and T. P. Russell, *Adv. Mater.*, 2015, **27**, 886-891.
11. Y. Galagan, F. Di Giacomo, H. Gorter, G. Kirchner, I. de Vries, R. Andriessen and P. Groen, *Adv. Energy Mater.*, 2018, **8**, 1801935.
12. S. Song, K. T. Lee, C. W. Koh, H. Shin, M. Gao, H. Y. Woo, D. Vak and J. Y. Kim, *Energy Environ. Sci.*, 2018, **11**, 3248-3255.
13. R. Sun, J. Guo, C. K. Sun, T. Wang, Z. H. Luo, Z. H. Zhang, X. C. Jiao, W. H. Tang, C. L. Yang, Y. F. Li and J. Min, *Energy Environ.Sci.*, 2019, **12**, 384-395.
14. J. Zhang, Y. Zhao, J. Fang, L. Yuan, B. Xia, G. Wang, Z. Wang, Y. Zhang, W. Ma, W. Yan, W. Su and Z. Wei, *Small*, 2017, **13**, 1700388.
15. N. Li and C. J. Brabec, *Energy Environ. Sci.*, 2015, **8**, 2902-2909.
16. Y. Cui, H. Yao, L. Hong, T. Zhang, Y. Xu, K. Xian, B. Gao, J. Qin, J. Zhang, Z. Wei and J. Hou, *Adv. Mater.*, 2019, 31, 1808356.
17. L. Zhang, X. B. Xu, B. J. Lin, H. Zhao, T. F. Li, J. M. Xin, Z. Z. Bi, G. X. Qiu, S. W. Guo, K. Zhou, X. W. Zhan and W. Ma, *Adv. Mater.*, 2018, **30**, 1805041.
18. Q. Kang, L. Ye, B. W. Xu, C. B. An, S. J. Stuard, S. Q. Zhang, H. F. Yao, H. Ade and J. H. Hou, *Joule*, 2019, **3**, 227-239.
19. Y. Wu, H. Yang, Y. Zou, Y. Y. Dong, J. Y. Yuan, C. H. Cui and Y. F. Li, *Energy Environ. Sci.*, 2019, **12**, 675-683.
20. L. Zhang, B. J. Lin, Z. F. Ke, J. Y. Chen, W. B. Li, M. J. Zhang and W. Ma, *Nano Energy*, 2017, **41**, 609-617.
21. W. W. Li, K. H. Hendriks, W. S. C. Roelofs, Y. Kim, M. M. Wienk and R. A. J. Janssen, *Adv. Mater.*, 2013, **25**, 3182-3186.
22. G. C. Zhang, R. X. Xia, Z. Chen, J. Y. Xiao, X. N. Zhao, S. Y. Liu, H. L. Yip and Y. Cao, *Adv. Energy Mater.*, 2018, **8**, 1801609.
23. B. Guo, W. B. Li, X. Guo, X. Y. Meng, W. Ma, M. J. Zhang and Y. F. Li, *Adv. Mater.*, 2017, **29**, 1702291.
24. G. C. Zhang, K. Zhang, Q. W. Yin, X. F. Jiang, Z. Y. Wang, J. M. Xin, W. Ma, H. Yan, F. Huang and Y. Cao, *J. Am. Chem. Soc.*, 2017, **139**, 2387-2395..
25. J. H. Carpenter, M. Ghasemi, E. Gann, I. Angunawela, S. J. Stuard, J. J. Rech, E. Ritchie, B. T. O'Connor, J. Atkin, W. You, D. M. DeLongchamp and H. Ade, *Adv. Funct. Mater.*, 2019, **29**, 1806977.
26. H. Sirringhaus, P. J. Brown, R. H. Friend, M. M. Nielsen, K. Bechgaard, B. M. W. Langeveld-Voss, A. J. H. Spiering, R. A. J. Janssen, E. W. Meijer, P. Herwig and D. M. de Leeuw, *Nature*, 1999, **401**, 685-688.
27. W. Li, M. Chen, J. Cai, E. L. K. Spooner, H. Zhang, R. S. Gurney, D. Liu, Z. Xiao, D. G. Lidzey, L. Ding and T. Wang, *Joule*, 2018, **3**, 819.
28. L. Zhang and W. Ma, *Chinese J. Polym. Sci.*, 2017, **35**, 184-197.
29. L. Ye, X. Jiao, M. Zhou, S. Zhang, H. Yao, W. Zhao, A. Xia, H. Ade and J. Hou, *Adv. Mater.*, 2015, **27**, 6046-6054.
30. H. A. Becerril, M. E. Roberts, Z. H. Liu, J. Locklin and Z. N. Bao, *Adv. Mater.* 2008, **20**, 2588.
31. L. Zhang, B. J. Lin, B. Hu, X. B. Xu and W. Ma, *Adv. Mater.*, 2018, **30**, 1800343.

32. M. J. Zhang, X. Guo, W. Ma, H. Ade and J. H. Hou, *Adv. Mater.*, 2015, **27**, 4655-4660.
33. W. C. Zhao, S. S. Li, H. F. Yao, S. Q. Zhang, Y. Zhang, B. Yang and J. H. Hou, *J. Am. Chem. Soc.*, 2017, **139**, 7148-7151.
34. S. Q. Zhang, Y. P. Qin, J. Zhu and J. H. Hou, *Adv. Mater.*, 2018, **30**, 1800868.
35. Q. P. Fan, W. Y. Su, Y. Wang, B. Guo, Y. F. Jiang, X. Guo, F. Liu, T. P. Russell, M. J. Zhang and Y. F. Li, *Sci. China Chem.*, 2018, **61**, 531-537.
36. Q. P. Fan, Y. Wang, M. J. Zhang, B. Wu, X. Guo, Y. F. Jiang, W. B. Li, B. Guo, C. N. Ye, W. Y. Su, J. Fang, X. M. Ou, F. Liu, Z. X. Wei, T. C. Sum, T. P. Russell and Y. F. Li, *Adv. Mater.*, 2018, **30**, 1704546.
37. Y. Liu, J. Zhao, Z. Li, C. Mu, W. Ma, H. Hu, K. Jiang, H. Lin, H. Ade and H. Yan, *Nat. Commun.*, 2014, **5**, 5293.
38. A. Hexemer, W. Bras, J. Glossinger, E. Schaible, E. Gann, R. Kirian, A. MacDowell, M. Church, B. Rude and H. Padmore, *J. Phys. Conf. Ser.*, 2010, **247**, 012007.
39. D. M. Smilgies, *J. Appl. Crystallogr.*, 2009, **42**, 1030-1034.
40. S. J. Ko, W. Lee, H. Choi, B. Walker, S. Yum, S. Kim, T. J. Shin, H. Y. Woo and J. Y. Kim, *Adv. Energy Mater.*, 2014, **5**, 1401687.
41. Z. A. Tan, S. S. Li, F. Z. Wang, D. P. Qian, J. Lin, J. H. Hou and Y. F. Li, *Sci. Rep.*, 2014, **4**, 4691.
42. J. A. Bartelt, D. Lam, T. M. Burke, S. M. Sweetnam and M. D. McGehee, *Adv. Energy Mater.*, 2015, **5**, 1500577.
43. S. S. Chen, Y. H. Liu, L. Zhang, P. C. Y. Chow, Z. Wang, G. Y. Zhang, W. Ma and H. Yan, *J. Am. Chem. Soc.*, 2017, **139**, 6298-6301.
44. S. S. Li, L. Ye, W. C. Zhao, X. Y. Liu, J. Zhu, H. Ade and J. H. Hou, *Adv. Mater.*, 2017, **29**, 1704051.
45. Y. P. Qin, M. A. Uddin, Y. Chen, B. Jang, K. Zhao, Z. Zheng, R. N. Yu, T. J. Shin, H. Y. Woo and J. H. Hou, *Adv. Mater.*, 2016, **28**, 9416.
46. A. K. K. Kyaw, D. H. Wang, V. Gupta, W. L. Leong, L. Ke, G. C. Bazan and A. J. Heeger, *ACS Nano*, 2013, **7**, 4569-4577.
47. T. Liu, Z. H. Luo, Q. P. Fan, G. Y. Zhang, L. Zhang, W. Gao, X. Guo, W. Ma, M. J. Zhang, C. L. Yang, Y. F. Li and H. Yan, *Energy Environ. Sci.*, 2018, **11**, 3275-3282.
48. E. Gann, A. T. Young, B. A. Collins, H. Yan, J. Nasiatka, H. A. Padmore, H. Ade, A. Hexemer and C. Wang, *Rev. Sci. Instrum.*, 2012, **83**, 045110.
49. Y. Wu, Z. Y. Wang, X. Y. Meng and W. Ma, *Prog. Chem.*, 2017, **29**, 93-101.
50. S. Mukherjee, C. M. Proctor, J. R. Tumbleston, G. C. Bazan, T. Q. Nguyen and H. Ade, *Adv. Mater.*, 2015, **27**, 1105-1111.
51. W. Ma, J. R. Tumbleston, M. Wang, E. Gann, F. Huang and H. Ade, *Adv. Energy Mater.*, 2013, **3**, 864-872.
52. B. P. Lyons, N. Clarke and C. Groves, *Energy Environ. Sci.*, 2012, **5**, 7657-7663.
53. X. D. Gu, L. Shaw, K. Gu, M. F. Toney and Z. N. Bao, *Nat. Commun.*, 2018, **9**, 534.
54. C. Luo, A. K. K. Kyaw, L. A. Perez, S. Patel, M. Wang, B. Grimm, G. C. Bazan, E. J. Kramer and A. J. Heeger, *Nano Lett.*, 2014, **14**, 2764.
55. J. Q. Mai, Y. Q. Xiao, G. D. Zhou, J. Y. Wang, J. S. Zhu, N. Zhao, X. W. Zhan and X. H. Lu, *Adv. Mater.*, 2018, **30**, 1802888.
56. H. Cha, S. Wheeler, S. Holliday, S. D. Dimitrov, A. Wadsworth, H. H. Lee, D. Baran, I. McCulloch and J. R. Durrant, *Adv. Funct. Mater.*, 2018, **28**, 1704389.

ARTICLE

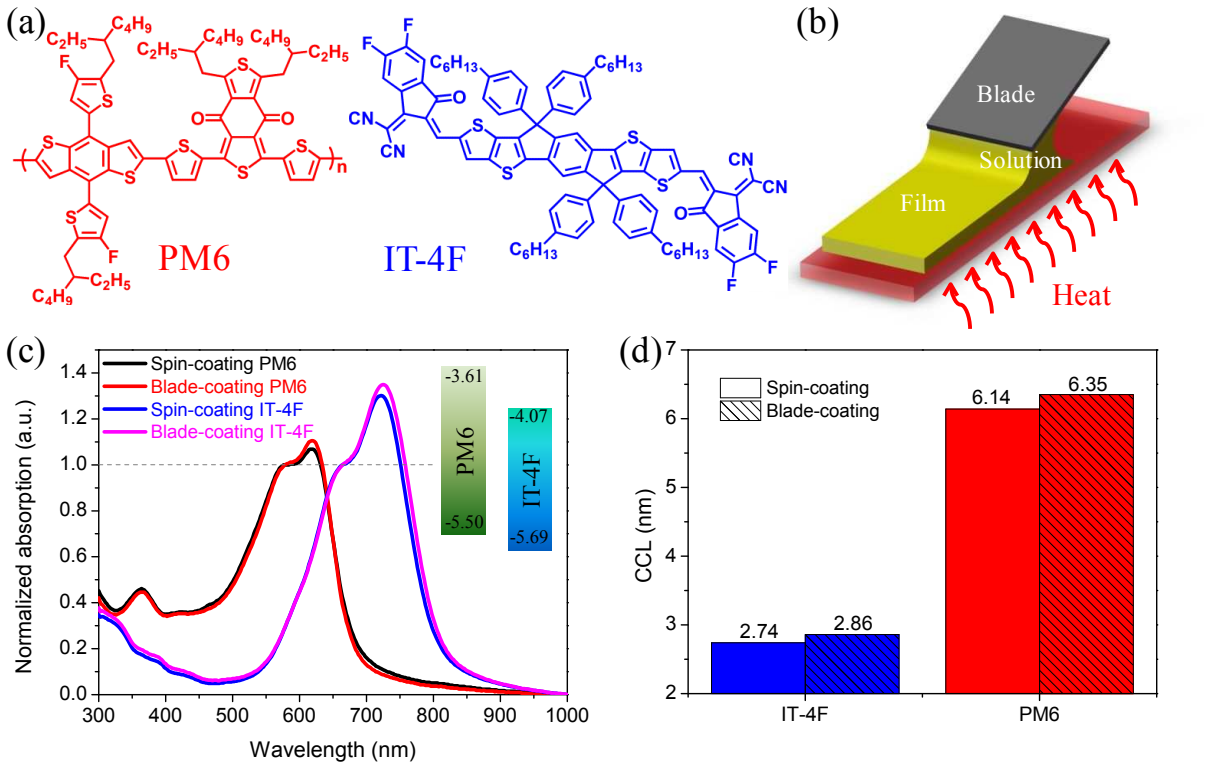

Fig. 1. (a) Chemical structures of PM6 and IT-4F. (b) The diagrammatic drawing of blade-coating with heating substrate. (c) The normalized UV-vis absorption spectra of PM6 and IT-4F films prepared by spin-coating and blade-coating (inset is the energy level of this system). All the speatra are normalized based on the intensity of 0-1 transition peaks (578 nm for PM6 and 664 nm for IT-4F) to highligth the variation of 0-0 transition peaks. (d) The calculated CCL values of (100) scattering peaks for PM6 and IT-4F films prepared by spin-coating and blade-coating.

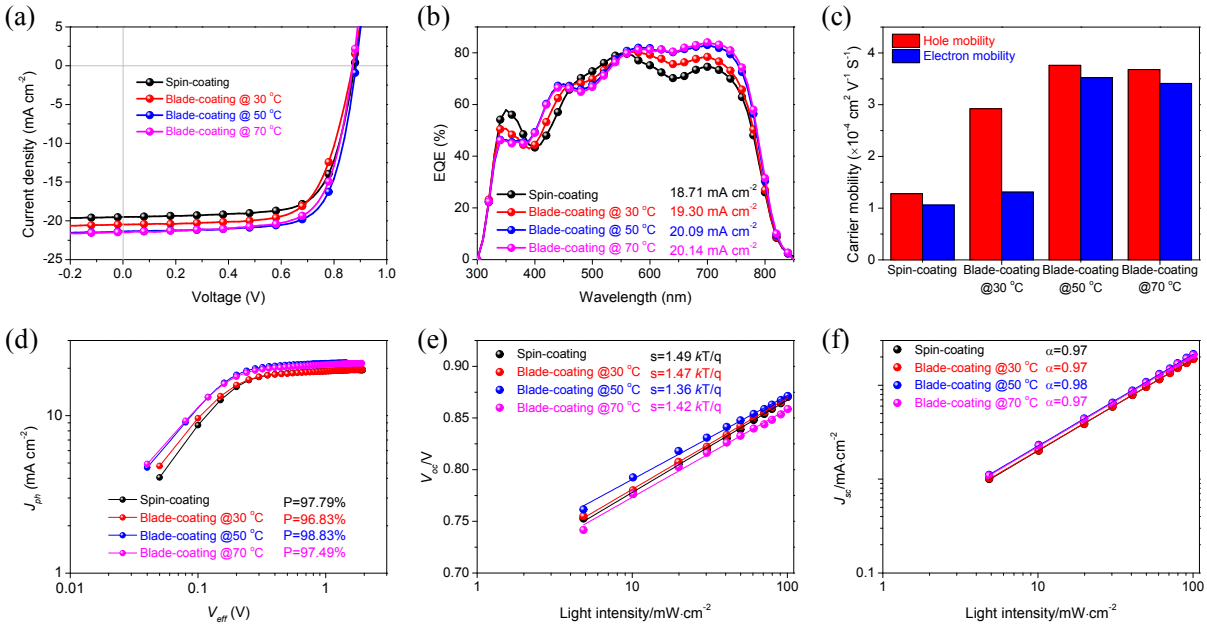

Fig. 2. (a) *J-V* curves, (b) EQE curves and (c) summarized carrier mobilities of the PM6:IT-4F devices. (d) J_{ph}-V_{eff} curves, (e) dependence of V_{oc} and (f) dependence of J_{sc} on light intensity for the PM6:IT-4F devices.

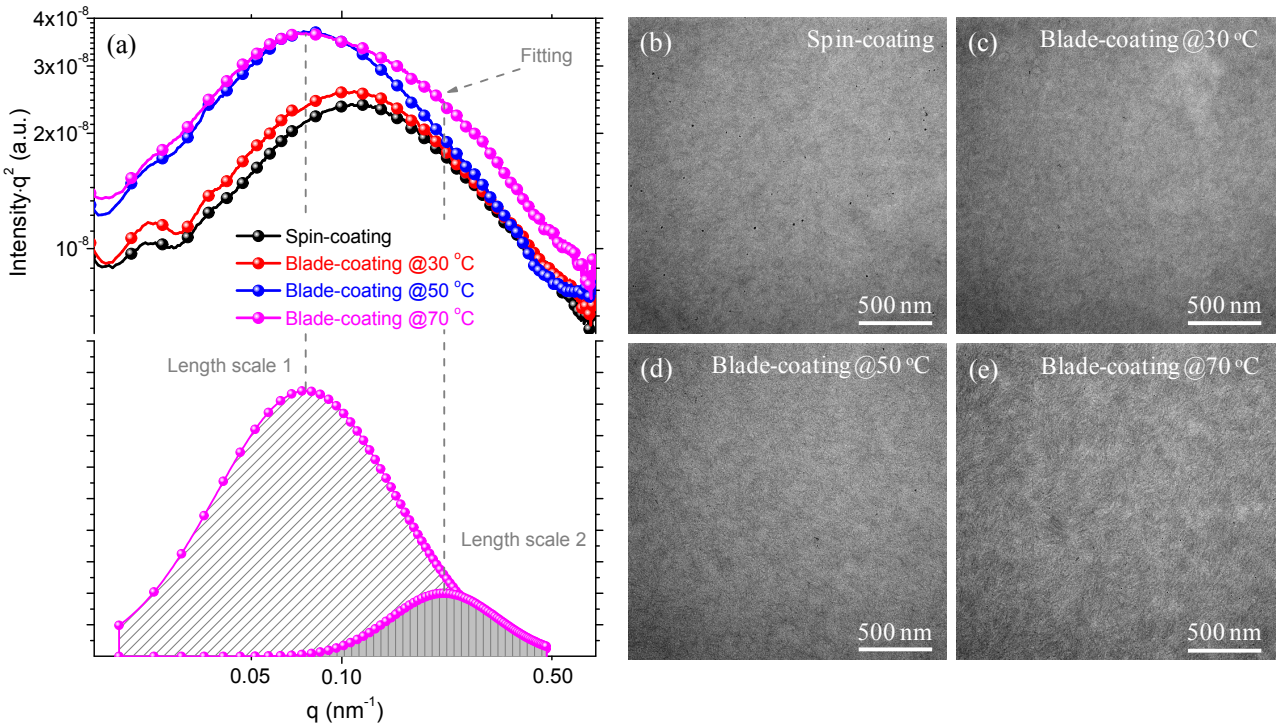

Fig. 3. (a) RSoXS profiles and (b-e) TEM images of PM6:IT-4F films.

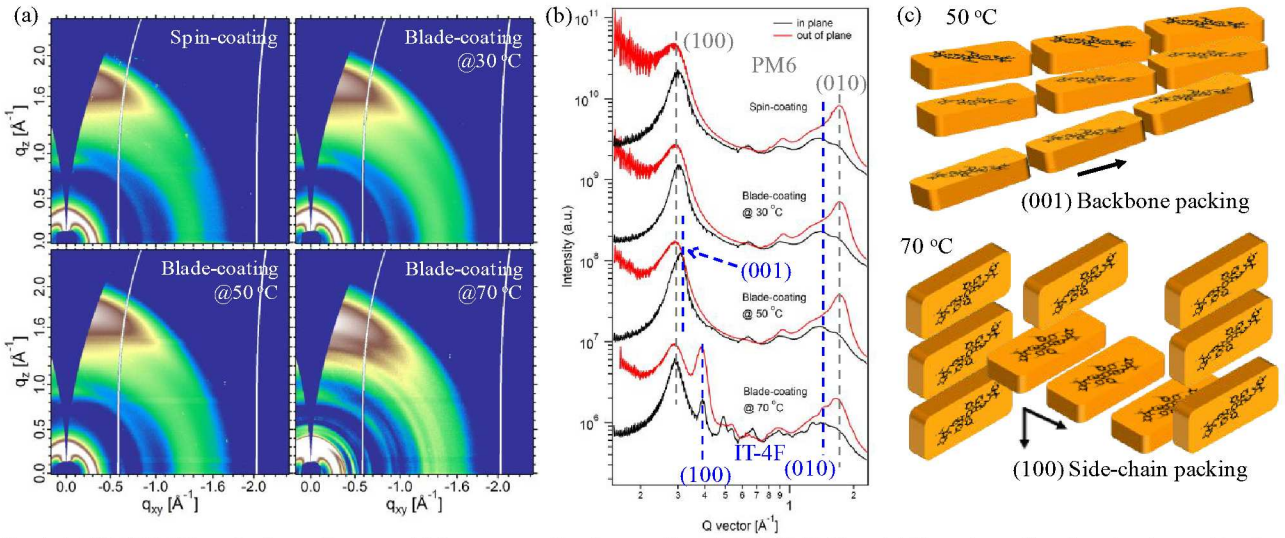

Fig. 4. (a) 2D GIWAXS scattering patterns and (b) corresponding line profiles of PM6:IT-4F films. (c) The schematics of molecular packing for IT-4F molecules in the blend films by blade-coating @ 50 °C and blade-coating @ 70 °C.

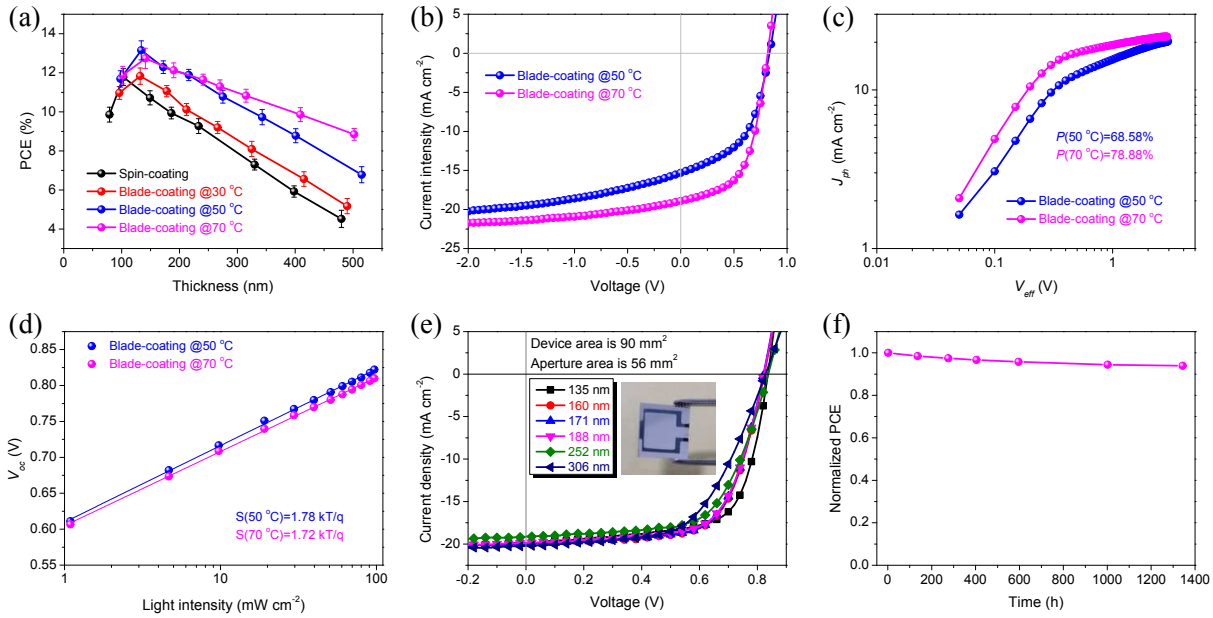

Fig. 5. (a) PCE values versus the thickness of active layer for PM6:IT-4F devices. (b) *J-V* curves, (c) J_{ph}-V_{eff} curves and d) dependence of V_{oc} on light intensity for PM6:IT-4F devices with thick films by blade-coating at the substrate temperature of 50 °C and 70 °C. (e) The *J-V* curves of blade-coated @70 °C large-area devices (device area is 90 mm^2 and the aperture area is 56 mm^2) with various thickness of active layer (inset is the image of large-area device). (f) The normalized PCE of blade-coated @70 °C devices with the increased time of storing in N_2-filled glovebox.

Table 1. Photovoltaic parameters of organic solar cells based on PM6:IT-4F blends by spin-coating and blade-coating under illumination of AM 1.5G, 100 mW cm^{-2}. (The effective device area is 4 mm^2. Average values are obtained from 15 devices)

	V_{oc} (V)	J_{sc} (mA cm^{-2})	FF (%)	PCE (%) (PCE_{max})	μ_h (cm^2 V^{-1} s^{-1})	μ_e (cm^2 V^{-1} s^{-1})
Spin-coating	0.88±0.01	18.99±0.52	70.47±0.81	11.78±0.43 (12.21)	1.28×10^{-4}	1.06×10^{-4}
Blade-coating @30 °C	0.87±0.01	19.89±0.59	68.39±0.62	11.83±0.42 (12.25)	2.92×10^{-4}	1.31×10^{-4}
Blade-coating @50 °C	0.88±0.01	20.76±0.61	72.00±0.55	13.15±0.49 (13.64)	3.76×10^{-4}	3.52×10^{-4}
Blade-coating @70 °C	0.87±0.01	20.84±0.63	70.18±0.71	12.74±0.52 (13.24)	3.68×10^{-4}	3.41×10^{-4}

Table 2. Phase separation parameters of PM6:IT-4F films obtained from RSoXS.

	Domain spacing[1] (nm)	Domain size[1] (nm)	Domain spacing[2] (nm)	Domain size[2] (nm)	Relative purity
Spin-coating	56	28	-	-	0.84
Blade-coating @30 °C	60	30	-	-	0.87
Blade-coating @50 °C	78	39	-	-	0.93
Blade-coating @70 °C	82	41	26	13	1

[1] is the length scale 1; [2] is the length scale 2.

Table 3. Structure parameters of PM6:IT-4F films obtained from GIWAXS.

	PM6 (100) in-plane		PM6 (100) out-of-plane		IT-4F (001) in-plane		IT-4F (100) in-plane	
	d_1 (nm)	CCL_1 (nm)	d_2 (nm)	CCL_2 (nm)	d_3 (nm)	CCL_3 (nm)	d_4 (nm)	CCL_4 (nm)
Spin-coating	2.09	10.66	2.17	9.27	-	-	-	-
Blade-coating @30 °C	2.09	12.03	2.17	9.76	-	-	-	-
Blade-coating @50 °C	2.17	16.62	2.17	10.30	2.03	19.49	-	-
Blade-coating @70 °C	2.17	13.24	2.17	10.70	-	-	1.61	26.91

Table of content

Blade-coated Highly Efficient Thick Active Layer of Non-fullerene Organic Solar Cells

Lin Zhang, [ab] Heng Zhao, [a] Baojun Lin, [a] Jian Yuan, [a] Xianbin Xu, [a] Jingnan Wu, [b] Ke Zhou, [a] Xia Guo, [b] Maojie Zhang [b] and Wei Ma*[a]

Highly efficient Large-area thick-film organic solar cells were fabricated by blade-coating with finely controlling the molecular packing.